ATLAS NOTE

ATLAS-CONF-2012-077

July 3, 2012

Search for direct production of charginos and neutralinos in events with three leptons and missing transverse momentum in $\sqrt{s} = 7$ TeV pp collisions with the ATLAS detector

The ATLAS Collaboration

ATLAS-CONF-2012-077
06 July 2012

Abstract

A search for the direct production of charginos and neutralinos in final states with three electrons or muons and missing transverse momentum is presented. The analysis is based on 4.7 fb^{-1} of $\sqrt{s} = 7$ TeV proton-proton collision data delivered by the Large Hadron Collider and recorded with the ATLAS detector. Observations are consistent with Standard Model expectations in three signal regions that are either depleted or enriched in Z-boson decays. Upper limits at 95% confidence level are set in R-parity conserving phenomenological minimal supersymmetric models and in simplified models, significantly extending previous results.

1 Introduction

Supersymmetry (SUSY) [1–9] postulates the existence of SUSY particles, or "sparticles", with spin differing by one-half unit with respect to that of their Standard Model (SM) partner. If R-parity [10–14] is conserved, the lightest SUSY particle (LSP) is stable and sparticles can only be pair-produced and decay into final states with SM particles and LSPs. Charginos ($\tilde{\chi}_i^{\pm}$, $i = 1, 2$) and neutralinos ($\tilde{\chi}_j^0$, $j = 1, 2, 3, 4$) are the mass eigenstates formed from the linear superposition of the SUSY partners of the Higgs and electroweak gauge bosons. These are the Higgsinos, and the winos, zino, and bino, collectively known as gauginos. Naturalness requires $\tilde{\chi}_i^{\pm}$ and $\tilde{\chi}_j^0$ (and third generation sparticles) to have masses in the hundreds of GeV range [15]. In scenarios where squark and gluino masses are larger than a few TeV, the direct production of gauginos may be the dominant SUSY process at the Large Hadron Collider (LHC). Charginos can decay into leptonic final states via sneutrinos ($\tilde{\nu}\ell^{\pm}$), sleptons ($\tilde{\ell}\nu$) or W bosons ($W\tilde{\chi}_1^0$), while unstable neutralinos can decay via sleptons ($\ell\tilde{\ell}^{\pm}$) or Z bosons ($Z\tilde{\chi}_1^0$).

This document presents a search with the ATLAS detector for the direct production of charginos and neutralinos decaying to a final state with three leptons (electrons or muons) and missing transverse momentum, the latter originating from the two undetected LSPs and the neutrinos. The analysis is based on 4.7 fb^{-1} of proton-proton collision data delivered by the LHC at a center-of-mass energy $\sqrt{s} = 7$ TeV between March and October 2011. The search described here significantly extends the current mass limits on charginos and neutralinos set by ATLAS [16, 17] and CMS [18]. Similar searches have been conducted at Tevatron [19, 20] and LEP [21], where a model independent limit of 103.5 GeV was set at 95% confidence limit (CL) on the mass of promptly decaying charginos.

2 Detector Description

ATLAS [22] is a multipurpose particle detector with forward-backward symmetric cylindrical geometry. It includes an inner tracker (ID) immersed in a 2 T magnetic field providing precision tracking of charged particles for pseudorapidities $|\eta| < 2.5$ [23]. Calorimeter systems with either liquid argon or scintillating tiles as the active media provide energy measurements over the range $|\eta| < 4.9$. The muon detectors are positioned outside the calorimeters and are contained in an air-core toroidal magnetic field produced by super conducting magnets with field integrals varying from 1 to 8 T·m. They provide trigger and high-precision tracking capabilities for $|\eta| < 2.4$ and $|\eta| < 2.7$, respectively.

3 New Physics Scenarios

In this analysis, observations are interpreted in the phenomenological minimal supersymmetric SM (pMSSM [24]) and in simplified models [25]. Additional interpretations of the results in the context of minimal universal extra dimensions (mUED [26]) and general gauge mediated SUSY (GGM [27,28]) models are provided in Appendix A.

In the pMSSM the mixing for the $\tilde{\chi}_i^{\pm}$ and $\tilde{\chi}_j^0$ depends on the gaugino masses M_1 and M_2, the Higgs mass parameter μ, and $\tan\beta$, the ratio of the expectation values of the two Higgs doublets. The dominant gauginos production leading to three-lepton final states is $\tilde{\chi}_1^{\pm}\tilde{\chi}_2^0$ production via the s-channel exchange of a virtual gauge boson. Other $\tilde{\chi}_i^{\pm}\tilde{\chi}_j^0$ processes contribute to a maximum of 20% to three-lepton final states depending on the values of the mass parameters. The right-handed sleptons (including third-generation sleptons) are assumed to be degenerate and have a mass $m_{\tilde{\ell}_R} = (m_{\tilde{\chi}_2^0} + m_{\tilde{\chi}_1^0})/2$, set via the right-handed SUSY-breaking slepton mass parameter at the electro-weak scale. In these scenarios, decays to sleptons are favored. The parameter $\tan\beta$ is set to 6, yielding comparable branching ratios into each slepton generation. The masses of the gluinos, squarks and left-handed sleptons are chosen to be larger than

2 TeV. The trilinear couplings are all set to zero, except for the stop sector, which is designed to achieve maximum mixing and thus a large Higgs mass.

In simplified models, the masses of the relevant particles ($\tilde{\chi}_1^{\pm}$, $\tilde{\chi}_2^0$, $\tilde{\chi}_1^0$, $\tilde{\nu}$, $\tilde{\ell}_L$) are the only free parameters. The charginos and heavy neutralinos are set to be wino-like and mass degenerate, and the lightest neutralino is set to be bino-like. The $\tilde{\chi}_1^{\pm}$ and $\tilde{\chi}_2^0$ are pair-produced and decay via left-handed sleptons, including staus, and sneutrinos of mass $m_{\tilde{\nu}} = m_{\tilde{\ell}_L} = (m_{\tilde{\chi}_1^0} + m_{\tilde{\chi}_1^{\pm}})/2$) with a branching ratio of 50% each.

4 Monte Carlo simulation

Several Monte Carlo (MC) generators are used to simulate SM processes and new physics signals relevant for this analysis. SHERPA [29] is used to simulate diboson processes WZ and ZZ. These include all diagrams leading to three leptons and one neutrino, and to four leptons respectively, including internal conversions (virtual photons converting into lepton pairs). HERWIG [30] is used for WW, while MadGraph [31] is used for the $t\bar{t}W$, $t\bar{t}WW$, $t\bar{t}Z$, $W\gamma$ and $Z\gamma$ processes. MC@NLO [32] is chosen for the simulation of single and pair production of top quarks, and ALPGEN [33] is used to simulate W/Z+jets. Expected diboson yields are normalized using next-to-leading order (NLO) QCD predictions obtained with MCFM [34, 35]. The top-quark pair-production contribution is normalized to approximate next-to-next-to-leading order calculations (NNLO) [36] and the $t\bar{t}W(W)/Z$ contributions are normalized to NLO results in agreement with the latest calculation within the quoted systematic uncertainties [37, 38]. The $W\gamma$ and $Z\gamma$ samples are normalized to the LO cross-sections from the MadGraph generator and an uncertainty is assigned to account for the difference between LO and NLO. The QCD NNLO FEWZ [39,40] cross-sections are used for normalization of the inclusive Z+light-flavor jets. The ratio of the NNLO to LO cross-section is used to rescale the Z+heavy-flavor jets LO cross-sections.

The choice of the parton distribution functions (PDFs) depends on the generator. The CTEQ6L1 [41] PDFs are used with MadGraph and ALPGEN, and the CT10 [42] PDFs with MC@NLO and SHERPA. The MRTSmcal PDF set [43] is used for HERWIG.

The pMSSM samples are produced with HERWIG and the simplified model samples with HERWIG++ [44]. The yields of the SUSY samples are normalized to the NLO cross-sections obtained from PROSPINO [45] using the PDF set CTEQ6.6 with the renormalization/factorization scales set to the average of the relevant gaugino masses.

Fragmentation and hadronization for the ALPGEN and MC@NLO (MadGraph) samples are performed with HERWIG (PYTHIA [46]), while for SHERPA, this is performed internally. For all MC samples, the propagation of particles through the ATLAS detector is modeled using GEANT4 [47, 48]. The effect of multiple proton-proton collisions in a bunch crossing is incorporated into the simulation by overlaying additional minimum bias events onto hard scatter events using PYTHIA. Simulated events are weighted to match the distribution of the mean number of interactions per bunch crossing observed in data.

5 Event Reconstruction and Preselection

The data sample was collected with an inclusive selection of a single-muon trigger (p_{T}^{μ}>18 GeV), a single-electron trigger (E_{T}^{e}>20 or 22 GeV, depending on the instantaneous luminosity), a di-muon trigger (p_{T}^{μ}>10 GeV), a di-electron trigger (E_{T}^{e}>12 GeV), and a e-μ trigger (E_{T}^{e}>10 GeV and p_{T}^{μ}>6 GeV, only used for 75% of data collected). For single lepton triggers at least one lepton is requested to have p_{T} (E_{T}) above 20 GeV (25 GeV) for muons (electrons); for di-lepton triggers at least two leptons are requested to have $p_{\mathrm{T}}(\mu,\mu)$>12,12 GeV, $E_{\mathrm{T}}(e,e)$>17,17 GeV or $E_{\mathrm{T}}(e)$, $p_{\mathrm{T}}(\mu)$>15,10 GeV. The p_{T} (E_{T}) thresholds are are chosen such that the overall trigger efficiency is high, typically in excess of 90%, and independent of the transverse momentum of the triggerable objects within uncertainties.

Events recorded during normal running conditions are analyzed if the primary vertex has five or more tracks associated to it. The primary vertex of an event is identified as the vertex with the highest Σp_{T} of associated tracks. Events containing jets failing the quality criteria described in Ref. [49] are rejected to suppress both SM and beam-induced background. Events containing muons candidates having transverse impact parameter with respect to the primary vertex $|d_0| > 0.2$ mm or longitudinal impact parameter with respect to the primary vertex $|z_0| > 1$ mm are rejected to suppress cosmic muon background.

Electrons must satisfy *tight* identification criteria [50] and fulfill $|\eta| < 2.47$ and $E_{\mathrm{T}} > 10$ GeV, where $|\eta|$ and E_{T} are determined from the calibrated clustered energy deposits in the electromagnetic calorimeter and the matched ID track respectively. Muons are reconstructed by combining tracks in the ID and tracks in the muon spectrometer [51]. Reconstructed muons are considered as candidates if they have transverse momentum $p_{\mathrm{T}} > 10$ GeV and $|\eta| < 2.4$.

"Tagged" leptons are electrons and muons, well separated from each other and from candidate jets. "Signal leptons" are tagged leptons for which the scalar sum of the transverse momenta of tracks within a cone $\Delta R \equiv \sqrt{(\Delta\phi)^2 + (\Delta\eta)^2} < 0.2$ around the lepton candidate, and excluding the lepton candidate track itself, is less than 10% of the E_{T} for electrons and less than 1.8 GeV for muons. Tracks selected for the electron and muon isolation requirement defined above have $p_{\mathrm{T}} > 1$ GeV and are associated to the primary vertex of the event. To suppress leptons originating from secondary vertices, the distance of closest approach of the lepton track to the primary vertex, normalized to its uncertainty is requested to be small, $|d_0|/\sigma(d_0) < 6(3)$ for electrons (muons).

Jets are reconstructed with the anti-k_t algorithm [52] with a radius parameter of $R = 0.4$ using clustered energy deposits calibrated at the electromagnetic scale. The jet energy is corrected to account for the non-compensating nature of the calorimeter using correction factors obtained from MC simulation and parameterized as a function of the jet E_{T} and η [49]. Jets considered in this analysis have $E_{\mathrm{T}} > 20$ GeV, $|\eta| < 2.5$ and a fraction of the jet's track momenta that can be associated with the primary vertex above 0.75. Jets are identified as containing b-hadron decays, and thus called "b-tagged", using a multivariate technique based on quantities such as the impact parameter of the tracks associated to the secondary vertex and the tracks in the jet, consistent with the expected topology of b-quark decays. The b-tagging algorithm [53] correctly identifies b-quark jets in simulated top decays with an efficiency of 60% and misidentifies jets containing light flavor quarks and gluons with a rate of $< 1\%$, for jets with $|\eta| < 2.5$ and jet $E_{\mathrm{T}} > 20$ GeV.

The missing transverse momentum, $E_{\mathrm{T}}^{\mathrm{miss}}$, is the magnitude of the vector sum of the transverse momentum or transverse energy of all $p_{\mathrm{T}} > 10$ GeV muons, $E_{\mathrm{T}} > 20$ GeV electrons, $E_{\mathrm{T}} > 20$ GeV jets, and calibrated calorimeter clusters with $|\eta| < 4.9$ not associated to these objects [54].

6 Signal Region Selection

Selected events must contain exactly three signal leptons. As leptonic decays of $\tilde{\chi}_j^0$ yield same-flavor opposite-sign (SFOS) lepton pairs, the presence of at least one such pair is required. The invariant mass of any SFOS lepton pair must be above 20 GeV to suppress background from low mass resonances and the missing transverse momentum must satisfy $E_{\mathrm{T}}^{\mathrm{miss}} > 75$ GeV.

Three signal regions are then defined: two "Z-depleted" regions (SR1a and SR1b), with no SFOS pairs having invariant mass within 10 GeV of the nominal Z-boson mass; and a "Z-enriched" one (SR2), where at least one SFOS pair has an invariant mass within 10 GeV of the Z-boson mass. Events in SR1a and SR1b are further required to contain no b-tagged jets to suppress contributions from b-jet-rich backgrounds, where a fake lepton could originate from a heavy-flavor decay. SR1b is designed to increase sensitivity to new physics with large mass splittings by requiring all three leptons to have $p_{\mathrm{T}} > 30$ GeV. In both SR1b and SR2, the transverse mass m_{T}, using the $E_{\mathrm{T}}^{\mathrm{miss}}$ and the lepton not forming the best Z candidate, must satisfy $m_{\mathrm{T}} > 90$ GeV. The m_{T} requirement is introduced to suppress background

Table 1: The selection requirements for the three signal regions. The Z-veto (request) rejects (selects) events with m_{SFOS} within 10 GeV of the Z-mass (91.2 GeV). The m_{T} is calculated from the $E_{\mathrm{T}}^{\mathrm{miss}}$ and the lepton not forming the best Z candidate.

Selection	SR1a	SR1b	SR2
Targeted Intermediate Decay	$\tilde{l}^{(*)}$ or Z^*		on-shell Z
N leptons (e, μ)	Exactly 3		
Lepton charge, flavour	At least one SFOS pair with $m_{\ell\ell} > 20$ GeV		
$E_{\mathrm{T}}^{\mathrm{miss}}$	> 75 GeV		
m_{SFOS}	Z-veto	Z-veto	Z request
N b-jets	0	0	any
m_{T}	any	> 90 GeV	> 90 GeV
p_{T} ℓ_3	> 10 GeV	> 30 GeV	> 10 GeV

from WZ. The SR1a/b regions target neutralino decays via intermediate sleptons or via off-shell Z-bosons while SR2 targets decays via an on-shell Z-boson. Table 1 summarizes the selection requirements for the three signal regions.

7 Standard Model Background Estimation

7.1 Reducible Background Processes

Several SM processes contribute to the background in the signal regions. A "reducible" process has at least one "fake" object, that is either a lepton from a semileptonic decay of a heavy-flavor quark or an electron from an isolated photon conversion. The contribution from misidentified light-flavor quark or gluon jets is negligible in the signal regions. The reducible background includes single- and pair-production of top-quark and WW or W/Z produced in association with jets or photons. The dominant component is the production of top quarks, with a contribution of 1% or less from Z+jets. The reducible background is estimated using a "matrix method" similar to that described in Ref. [55].

In this implementation of the matrix method, the signal lepton with the highest p_{T} or E_{T} is taken to be real, which is a valid assumption in 99% of the cases, based on MC studies. The number of observed events with one or two fakes is then extracted from a system of linear equations relating the number of events with two additional signal or tagged candidates to the number of events with two additional candidates that are either real or fake. The coefficients of the linear equations are functions of the real lepton identification efficiencies and of the fake object misidentification probabilities.

The identification efficiency is measured in data using lepton candidates from $Z \rightarrow \ell\ell$ decays. Misidentification probabilities for each relevant fake type (heavy flavor, conversion) and for each reducible background process are obtained using simulated events with one signal and two tagged leptons. These misidentification probabilities are then corrected using the ratio (fake scale factor) of the misidentification probability in data and that in MC simulation obtained in dedicated control samples. For heavy flavor fakes, the correction factor is measured in a $b\bar{b}$ dominated control sample. This is defined by selecting events with only one b-tagged jet (containing a muon) and a tagged lepton, for which the fake rate is measured. The non-$b\bar{b}$ background includes top pair production and W produced in association with a b-quark. An $E_{\mathrm{T}}^{\mathrm{miss}}$ requirement of less than 40 GeV suppresses both the $t\bar{t}$ and the W contamination, while requesting $m_{\mathrm{T}} < 40$ GeV reduces the W background. The remaining (small) background is subtracted from data using MC predictions. The fake scale factor for the conversion candidates is determined in a sample of photons radiated from a muon in $Z \rightarrow \mu\mu$ decays. These are selected by requesting $M_{\mu\mu e}$ to lie within 10 GeV of the nominal Z-boson mass value. A weighted average misidentification

Table 2: Expected numbers of events from SM backgrounds (Bkg.) and observed numbers of events in data, for 4.7 fb^{-1}, in validation regions VR1, VR2 and VR3. Both statistical and systematic uncertainties are included.

Selection	VR1	VR2	VR3
$t\bar{t}Z$	0.17±0.14	0.12±0.10	1.1±0.9
$t\bar{t}W$	0.6±0.5	0.7±0.5	0.10±0.08
$t\bar{t}WW$	0.017±0.014	0.022±0.017	0.0023±0.0019
ZZ	17±15	0.10±0.05	3.9±0.6
WZ	46±8	0.93±0.29	98±12
Reducible Bkg.	50±28	13±7	$3.1^{+4.7}_{-3.1}$
Total Bkg.	114±32	15±7	106±13
Data	126	18	109

probability is then calculated by weighting the corrected type- and process-dependent misidentification probabilities according to the relative contributions in a given region.

7.2 Irreducible Background Processes

A background process is considered "irreducible" if it leads to events with three real and isolated leptons, referred to as "real" leptons below. These include diboson (WZ and ZZ) and $t\bar{t}W/Z$ production, where the gauge boson may be produced off-mass-shell. The ZZ and $t\bar{t}W/Z$ contribution is determined using the corresponding MC samples, for which lepton and jet selection efficiencies are corrected to account for differences with respect to data.

The largest irreducible background, WZ, is determined using a semi-data-driven approach. The WZ background is fit to data in a control region including events with exactly three leptons, one SFOS lepton pair, a Z candidate, $E_{\mathrm{T}}^{\mathrm{miss}} < 50$ GeV, a b-veto, and $m_T(W) > 40$ GeV. The WZ purity after all above cuts in the control region is ~80%. Non-WZ backgrounds, both irreducible and reducible, are determined based on MC or by using the matrix method and subtracted. A WZ normalization factor 1.25±0.12 is obtained in the control region under a background-only hypothesis and used to estimate the WZ in the validation regions. To obtain the model-independent 95% CL upper limit on the new physics cross-section, a fit is performed simultaneously in the WZ control region and in the signal region, with floating WZ normalization factor and a non-negative new physics signal in the signal region only. This allows the propagation of the uncertainties on the normalization factor. When setting limits on specific new physics scenarios, the potential signal contamination in the WZ control region is accounted for in the simultaneous fit.

8 Background Model Validation

The background predictions have been tested in various validation regions. A Drell-Yan and WZ dominated region (VR1) includes events with three signal leptons, at least one SFOS lepton pair, $30 < E_{\mathrm{T}}^{\mathrm{miss}} < 75$ GeV, and satisfying a Z-boson veto. A reducible background dominated region (VR2, where top pair-production and decay to two real and one fake lepton is the main contribution) is built by requiring three signal leptons, $E_{\mathrm{T}}^{\mathrm{miss}} > 50$ GeV and by veto-ing SFOS lepton pairs. Finally, a WZ dominated region (VR3) is defined by selecting events with three signal leptons, at least one a SFOS lepton pair, a Z candidate, and $50 < E_{\mathrm{T}}^{\mathrm{miss}} < 75$ GeV. The data and predictions are in agreement within the quoted statistical and systematic uncertainties as shown in Table 2 and distributions are presented in Appendix A.

9 Systematic uncertainties

Several sources of systematic uncertainty are considered in the signal, control and validation regions. The systematic uncertainties affecting the MC based estimates (the yield of the irreducible background, the cross-section weighted misidentification probabilities, the signal yield) include the theoretical cross section uncertainties due to renormalisation and factorisation scale and PDFs, the acceptance uncertainty due to PDFs, the uncertainty due to the choice of MC generator, jet energy scale, jet energy resolution, lepton energy scale, lepton energy resolution, lepton efficiency, b-tagging efficiency and mistag probability, and the uncertainty on the luminosity. In SR1a, the total uncertainty on the irreducible background is 24%. This is dominated by the uncertainty on the efficiency of the signal regions' selection for the WZ generator, determined by comparing the nominal yield with that obtained with the `HERWIG` generator and found to be 20%. The next largest uncertainties are the uncertainty on the cross sections (9%) and that due the MC generator uncertainty (1%) of the non-WZ background. The MC generator uncertainty partially accounts for the cross section uncertainty, leading to a slight overestimate of the overall uncertainty. All the remaining uncertainties on the irreducible background in this signal region range between 0.5–5%. The total uncertainty on the irreducible background in SR1b is slightly larger, at 25%, due to the limited number of simulated events. In SR2, the uncertainties on the irreducible background are 24%, with increased contributions from the jet energy scale and resolution and cross-section uncertainties.

The uncertainty on the reducible background includes the MC uncertainty on the weights for the misidentification probabilities from the sources listed above (up to 10%) and the uncertainty due to the dependence of the misidentification probability on $E_{\mathrm{T}}^{\mathrm{miss}}$ (0.6–15%). Also included in the uncertainty on the reducible background is the uncertainty on the fake scale factors (10–34%), and that due to the limited number of data events with three tagged leptons, of which at least one is a signal lepton (19–130%). The latter uncertainty is highest in SR2 where the reducible background is very low.

The total uncertainties on the signal yields are between 10–20%, where the largest contribution is from the uncertainty on the cross-sections at ~7%. Signal cross sections are calculated to NLO in the strong coupling constant using `PROSPINO`. An envelope of cross section predictions is defined using the 68% C.L. ranges of the `CTEQ6.6` [56] (including the α_S uncertainty) and `MSTW` [57] PDF sets, together with variations of the factorisation and renormalisation scales by factors of two or one half. The nominal cross section value is taken to be the midpoint of the envelope and the uncertainty assigned is half the full width of the envelope, closely following the PDF4LHC recommendations [58].

In all of the above, the value used for the uncertainty on the luminosity is 3.9% [59, 60]. Correlations of systematic uncertainties between processes and regions are accounted for.

10 Results and Interpretation

The numbers of observed events and the prediction for SM backgrounds in SR1a, SR1b and SR2 are reported in Table 3. Distributions of the $E_{\mathrm{T}}^{\mathrm{miss}}$ in SR1a and SR2 are presented in Fig. 1. Additional distributions are shown in Appendix A.

No significant excess of events is found in any of the three signal regions. Upper limits on the visible cross section, defined by the product of production cross section times acceptance times efficiency, of 3.0 fb in SR1a, 0.7 fb in SR1b and 2.0 fb in SR2 are placed at 95% CL with the modified frequentist CL_s prescription [61]. All systematic uncertainties and their correlations are taken into account via nuisance parameters in a profile likelihood fit [62]. The corresponding expected limits are 3.0 fb, 0.8 fb and 2.0 fb, respectively.

SR1a and SR1b provide the best sensitivity for the pMSSM scenarios, and the interpretations are shown in Fig. 2. In particular, SR1a (SR1b) target scenarios with small (large) mass splitting between the heavy gauginos and the LSP. The limits are calculated using - model point by model point - the signal

Table 3: Expected numbers of events from SM backgrounds (Bkg.) and observed numbers of events in data, for 4.7 fb^{-1}, in signal regions SR1a, SR1b and SR2. The yield for one of the simplified model scenarios, "SUSY ref. point", ($m_{\tilde{\chi}_1^\pm}, m_{\tilde{\chi}_2^0}, m_{\tilde{\ell}_L}, m_{\tilde{\chi}_1^0} = 425,\ 425,\ 250,\ 75$ GeV) is also presented. Both statistical and systematic uncertainties are included. Upper limits on the observed and expected visible production cross-section at 95% CL are also shown.

Selection	SR1a	SR1b	SR2
SUSY ref. point	8.0±0.8	6.5±0.6	0.46±0.05
$t\bar{t}Z$	0.06±0.05	0.025±0.023	0.6±0.5
$t\bar{t}W$	0.36±0.29	0.10±0.08	0.09±0.08
$t\bar{t}WW$	0.010±0.008	0.0023±0.0019	0.004±0.004
ZZ	0.67±0.21	0.09±0.08	0.34±0.17
WZ	13.5±3.2	1.1±0.28	9.3±2.2
Reducible Bkg.	10±5	0.35±0.34	$0.5^{+1.0}_{-0.5}$
Total Bkg.	25±6	1.6±0.5	10.9±2.4
Data	24	0	11
Visible σ (exp)	<3.0 fb	<0.8 fb	<2.0 fb
Visible σ (obs)	<3.0 fb	<0.7 fb	<2.0 fb

region providing the best expected limit. The uncertainties on the signal cross-section are not included in the limit calculation but their impact on the observed limit is shown. A large difference between expected and observed limits is seen in the upper right corner of the $M_1 = 100$ GeV slice of the pMSSM scenarios in Fig. 2, where SR1b has the best sensitivity. Lower M_1 values lead to sizable mass splittings between $\tilde{\chi}_1^\pm$ and $\tilde{\chi}_1^0$ and therefore to large acceptances. The production cross-section decreases as M_2 and μ increase, leading to a less stringent limit for high values of the two parameters. The search does not have sensitivity in the region at low M_2 and high μ due to the small mass splitting between the $\tilde{\chi}_2^0$ and the $\tilde{\chi}_1^0$. The value of $\tan\beta$ does not have a significant impact on $\sigma(pp \to \tilde{\chi}_i^\pm \tilde{\chi}_j^0) \times BR(\tilde{\chi}_i^\pm \tilde{\chi}_j^0 \to \ell\ell\ell\tilde{\chi}_1^0)$, which varies by ~10% if $\tan\beta$ is raised from 6 to 10. SR1b provides the best sensitivity to the simplified models for which the interpretation is shown in Fig. 3. In the simplified models considered, degenerate $\tilde{\chi}_1^\pm$ and $\tilde{\chi}_2^0$ masses up to 500 GeV are excluded for large mass differences from the $\tilde{\chi}_1^0$.

Results in SR1a are also interpreted in the mUED model, where small mass differences are expected, and results in SR2 are interpreted in a Z-rich GGM scenario (Appendix A).

11 Summary

Results from a search for direct production of charginos and neutralinos in the final state with three leptons (electrons or muons) and missing transverse momentum are reported. The analysis is based on 4.7 fb^{-1} of proton-proton collision data delivered by the LHC at $\sqrt{s}$ =7 TeV. No significant excess of events is found in data. The null result is interpreted in pMSSM and simplified models. For the simplified models considered in this paper, degenerate $\tilde{\chi}_1^\pm$ and $\tilde{\chi}_2^0$ masses up to 500 GeV are excluded for large mass differences from the $\tilde{\chi}_1^0$. Additional interpretations in mUED and GGM models are also provided.

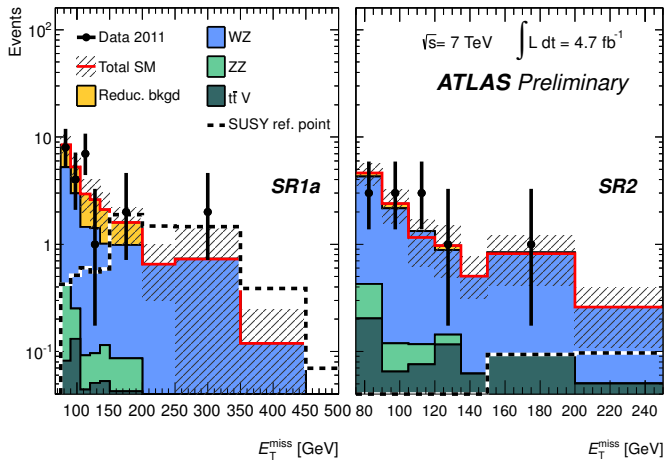

Figure 1: $E_{\mathrm{T}}^{\mathrm{miss}}$ distributions for events in signal regions SR1a (left) and SR2 (right). The uncertainty band includes both statistical and systematic uncertainty, while the uncertainties on the data points are statistical only. The yield for one of the simplified model scenarios, "SUSY ref. point", ($m_{\tilde{\chi}_1^\pm}, m_{\tilde{\chi}_2^0}, m_{\tilde{\ell}_L}, m_{\tilde{\chi}_1^0} = 425, 425, 250, 75$ GeV) is also shown for illustration purposes. For this SUSY ref. point, 8.0±0.8 events are expected in SR1a, 6.5±0.6 in SR1b and 0.46±0.05 in SR2. The expected yield for the SUSY ref. point is small in SR2 as this scenario is not rich in on-shell Z bosons.

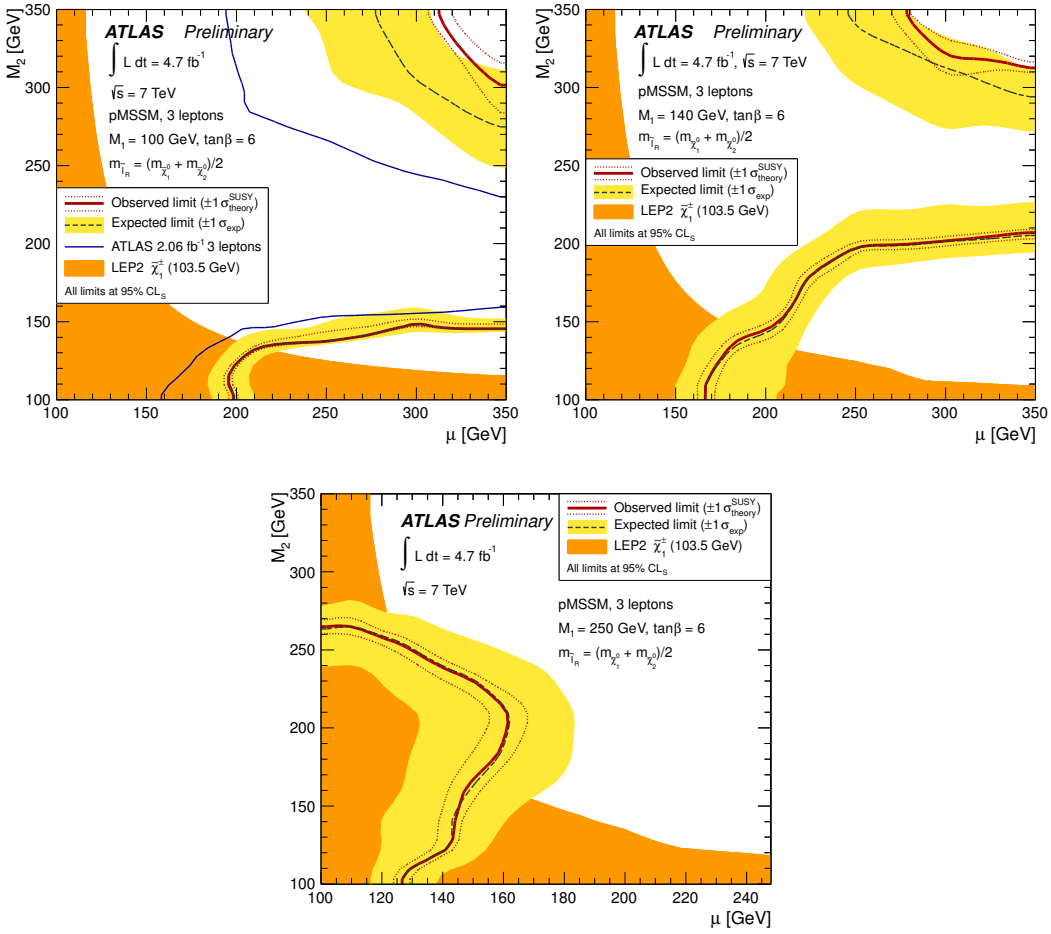

Figure 2: Observed and expected 95% CL limit contours for chargino and neutralino production in the pMSSM for $M_1 = 100$ GeV (top left), $M_1 = 140$ GeV (top right) and $M_1 = 250$ GeV (bottom). The regions with low values of M_2 and μ are the excluded ones for all values of $M_1 = 100$ GeV. The expected and observed limits are calculated without signal cross-section uncertainty taken into account. The yellow band is the $\pm 1\sigma$ experimental uncertainty on the expected limit. The red dashed band is the $\pm 1\sigma$ signal theory uncertainty on the observed limit. Linear interpolation is used to account for the discreteness of the signal grids. The exclusion contours are optimized by applying in each signal grid point the CL values from the most sensitive signal region (lowest expected CL) for $M_1 = 100$ GeV and 140 GeV. Signal region SR1a is used for $M_1 = 250$ GeV.

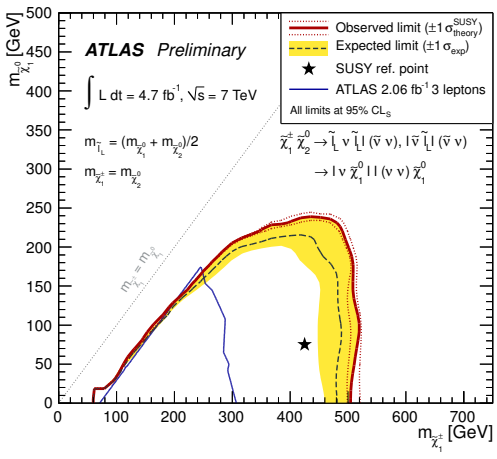

Figure 3: Observed and expected 95% CL limit contours for chargino and neutralino production in the simplified model scenario. The expected and observed limits are calculated without taking the signal cross-section uncertainty into account. The yellow band is the $\pm 1\sigma$ experimental uncertainty on the expected limit. The red dashed band is the $\pm 1\sigma$ signal theory uncertainty on the observed limit. Linear interpolation is used to account for the discreteness of the signal grids.

A Appendix: Additional Material

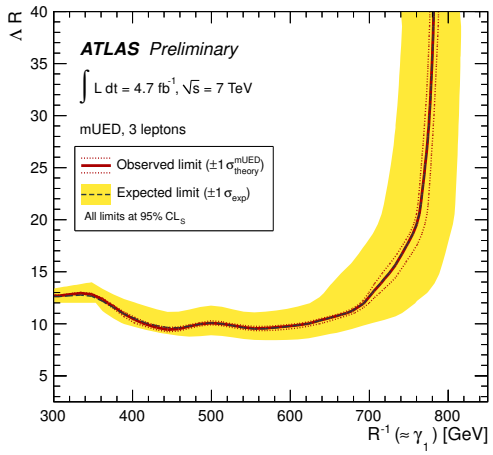

Figure 4: Observed and expected 95% CL limit contours for the minimal universal extra dimensions (mUED) model [26]. In the mUED model, one extra dimension is introduced that is compactified on a S^1/Z_2 orbifold with a characteristic lenght scale R and it is an effective theory valid up to a cutoff scale, Λ. The SM fields are allowed to propagate in the extra spatial dimension resulting in a Kaluza-Klein (KK) tower of excited SM particles. Conservation of momentum in the extra dimension gives rise to a conserved KK-number and leads to a phenomenology analogous to R-parity conserving SUSY: KK-particles are pair-produced and the lightest KK particle (typically the photon γ^*) is stable and neutral. The production of KK-particles is dominated by pair production of KK-quarks and KK-gluons that decay via excited KK-Ws and KK-Zs to multilepton final states with γ^* producing significant missing transverse momentum. The mUED signal samples are produced with, and normalized to the prediction from, the LO HERWIG++ generator. SR1a provides the best sensitivity to the mUED model, which tends to have soft leptons. The expected and observed limits are calculated without taking the signal cross-section uncertainty into account. The yellow band is the $\pm 1\sigma$ experimental uncertainty on the expected limit. The red dashed band is the $\pm 1\sigma$ signal theory uncertainty on the observed limit. Linear interpolation is used to account for the discreteness of the signal grids. The results from this search exclude $1/R$ values below 775 GeV for large values of ΛR, significantly extending current limits [63].

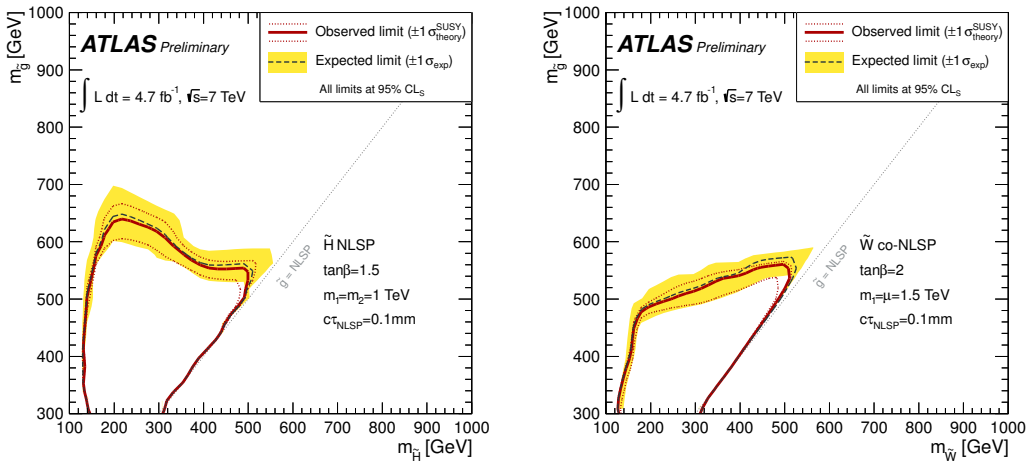

Figure 5: Observed and expected 95% CL limit contours for general gauge mediated SUSY models (GGM) [27, 28] with higgsino next-to-lightest SUSY particle (NLSP) (left) and wino co-NLSP (right). The GGM lightest SUSY particle is always a light gravitino ($\tilde{G}$). In GGM higgsino scenarios with a mass hierarchy $\mu \ll m_{1,2}$, the NLSP is the $\tilde{H}$ decaying via $\gamma\tilde{G}$ or $Z\tilde{G}$. The parameters are set to $m_1 = m_2 = 1$ TeV, $\tan\beta = 1.5$, and $c\tau_{NLSP} = 0.1$ mm. The μ term is required to be positive, but is within the bounds required for a $\tilde{H}$ NLSP. In the GGM wino scenarios with $m_2 \ll \mu, m_1$, the wino-like $\tilde{\chi}_1^{\pm}$ and $\tilde{\chi}_1^0$ are degenerate in mass and act as co-NLSP. The co-NLSPs then decay into $\gamma\tilde{G}$, $Z\tilde{G}$, and $W^{\pm}\tilde{G}$. The chosen parameters are $m_1 = \mu = 1.5$ TeV, $\tan\beta = 2$ and $c\tau_{NLSP} = 0.1$ mm. The mass m_2 is varied as required to produce the wino co-NLSP. The GGM signal samples are produced with `PYTHIA` and the sample yields normalized to the NLO+NLL cross sections and using the midpoint of the `CTEQ6.6` and `MSTW2008` PDF sets (see text for details). SR2 provides the best sensitivity in the Z-rich GGM models. The expected and observed limits are calculated without taking the signal cross-section uncertainty into account. The yellow band is the $\pm 1\sigma$ experimental uncertainty on the expected limit. The red dashed band is the $\pm 1\sigma$ signal theory uncertainty on the observed limit. Linear interpolation is used to account for the discreteness of the signal grids. In GGM higgsino NLSP models, gluinos are excluded with mass up to 600 GeV for low higgsino masses, strengthening current limits [64]. In GGM wino co-NLSP models, gluinos are excluded with mass up to 520 GeV for wino masses less than 480 GeV.

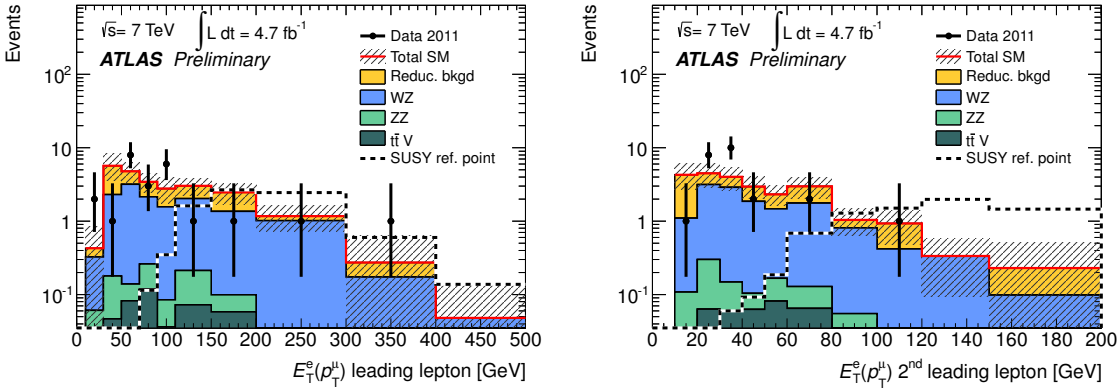

Figure 6: For events in SR1a, the p_{T} distributions of the leading (left) and sub-leading (right) lepton are shown for 2011 data and MC simulation. The grey hatched band represents statistical and systematic uncertainties added in quadrature. The yield for one of the simplified model scenarios, "SUSY ref. point", $(m_{\tilde{\chi}_1^\pm}, m_{\tilde{\chi}_2^0}, m_{\tilde{\ell}_L}, m_{\tilde{\chi}_1^0} = 425,\ 425,\ 250,\ 75\ \mathrm{GeV})$ is also shown for illustration purposes. For this SUSY ref. point, 8.0±0.8 events are expected in SR1a, 6.5±0.6 in SR1b and 0.46±0.05 in SR2. The expected yield for the SUSY ref. point is small in SR2 as this scenario is not rich in on-shell Z bosons.

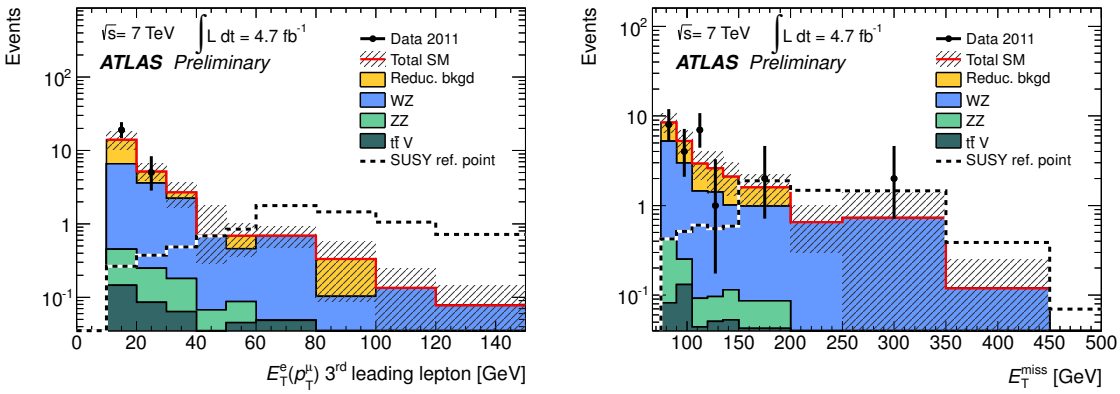

Figure 7: For events in SR1a, the p_{T} distribution of the third-leading lepton (left) and $E_{\mathrm{T}}^{\mathrm{miss}}$ distribution (right) are shown for 2011 data and MC simulation. The grey hatched band represents statistical and systematic uncertainties added in quadrature. The yield for one of the simplified model scenarios, "SUSY ref. point", $(m_{\tilde{\chi}_1^\pm}, m_{\tilde{\chi}_2^0}, m_{\tilde{\ell}_L}, m_{\tilde{\chi}_1^0} = 425,\ 425,\ 250,\ 75\ \mathrm{GeV})$ is also shown for illustration purposes. For this SUSY ref. point, 8.0±0.8 events are expected in SR1a, 6.5±0.6 in SR1b and 0.46±0.05 in SR2. The expected yield for the SUSY ref. point is small in SR2 as this scenario is not rich in on-shell Z bosons.

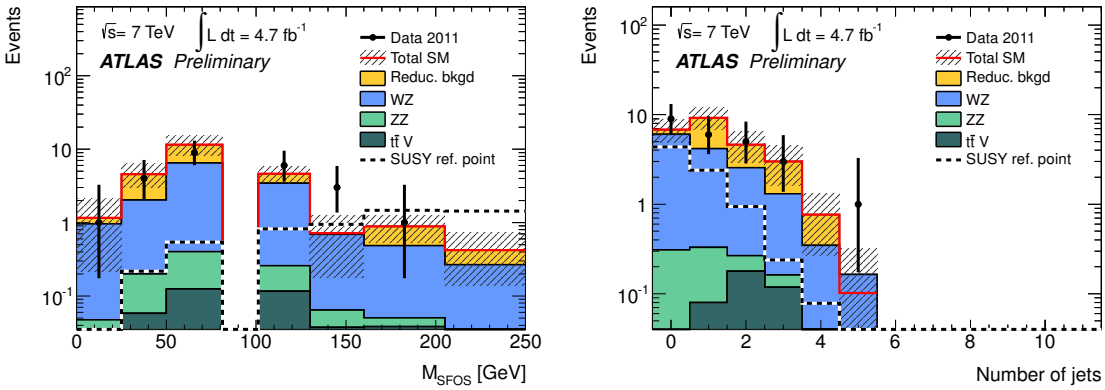

Figure 8: For events in SR1a, the m_{SFOS} (left) and jet multiplicity (right) distributions are shown for 2011 data and MC simulation. In events where multiple SFOS lepton pairs are present, the pair with invariant mass closest to the Z boson mass is plotted. The grey hatched band represents statistical and systematic uncertainties added in quadrature. The yield for one of the simplified model scenarios, "SUSY ref. point", $(m_{\tilde{\chi}_1^\pm}, m_{\tilde{\chi}_2^0}, m_{\tilde{\ell}_L}, m_{\tilde{\chi}_1^0} = 425, 425, 250, 75\,\mathrm{GeV})$ is also shown for illustration purposes. For this SUSY ref. point, 8.0±0.8 events are expected in SR1a, 6.5±0.6 in SR1b and 0.46±0.05 in SR2. The expected yield for the SUSY ref. point is small in SR2 as this scenario is not rich in on-shell Z bosons.

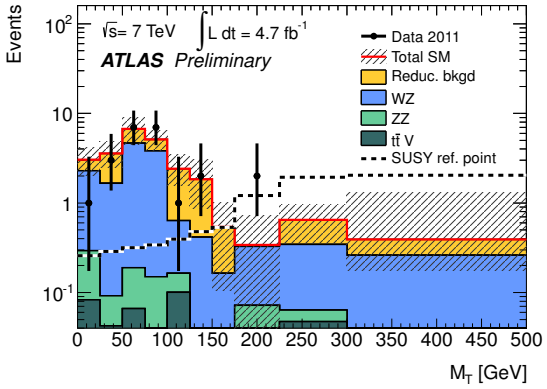

Figure 9: For events in SR1a, the m_{T} distribution is shown for 2011 data and MC simulation. The m_{T} is formed using the $E_{\mathrm{T}}^{\mathrm{miss}}$ and the lepton not forming the best Z candidate. The grey hatched band represents statistical and systematic uncertainties added in quadrature. The yield for one of the simplified model scenarios, "SUSY ref. point", $(m_{\tilde{\chi}_1^\pm}, m_{\tilde{\chi}_2^0}, m_{\tilde{\ell}_L}, m_{\tilde{\chi}_1^0} = 425, 425, 250, 75\,\mathrm{GeV})$ is also shown for illustration purposes. For this SUSY ref. point, 8.0±0.8 events are expected in SR1a, 6.5±0.6 in SR1b and 0.46±0.05 in SR2. The expected yield for the SUSY ref. point is small in SR2 as this scenario is not rich in on-shell Z bosons.

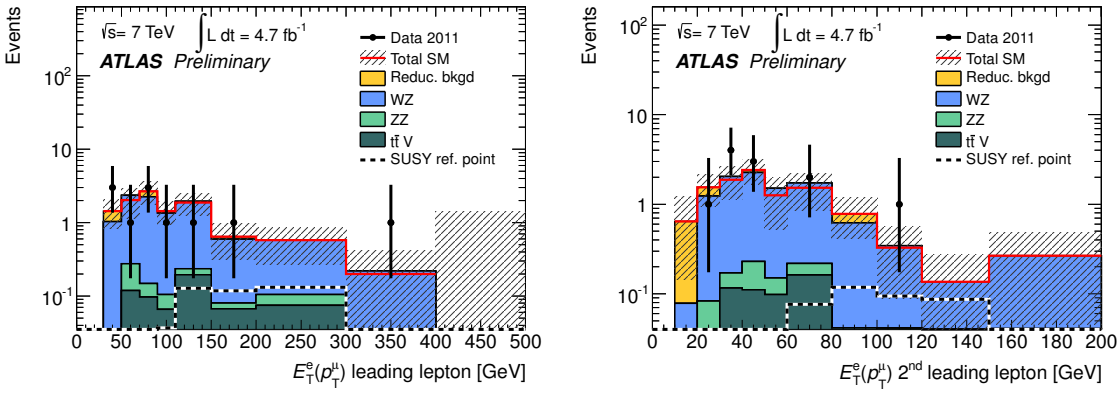

Figure 10: For events in SR2, the p_{T} distributions of the leading (left) and sub-leading (right) leptons are shown for 2011 data and MC simulation. The grey hatched band represents statistical and systematic uncertainties added in quadrature. The yield for one of the simplified model scenarios, "SUSY ref. point", $(m_{\tilde{\chi}_1^\pm}, m_{\tilde{\chi}_2^0}, m_{\tilde{\ell}_L}, m_{\tilde{\chi}_1^0} = 425,\ 425,\ 250,\ 75\ \mathrm{GeV})$ is also shown for illustration purposes. For this SUSY ref. point, 8.0±0.8 events are expected in SR1a, 6.5±0.6 in SR1b and 0.46±0.05 in SR2. The expected yield for the SUSY ref. point is small in SR2 as this scenario is not rich in on-shell Z bosons.

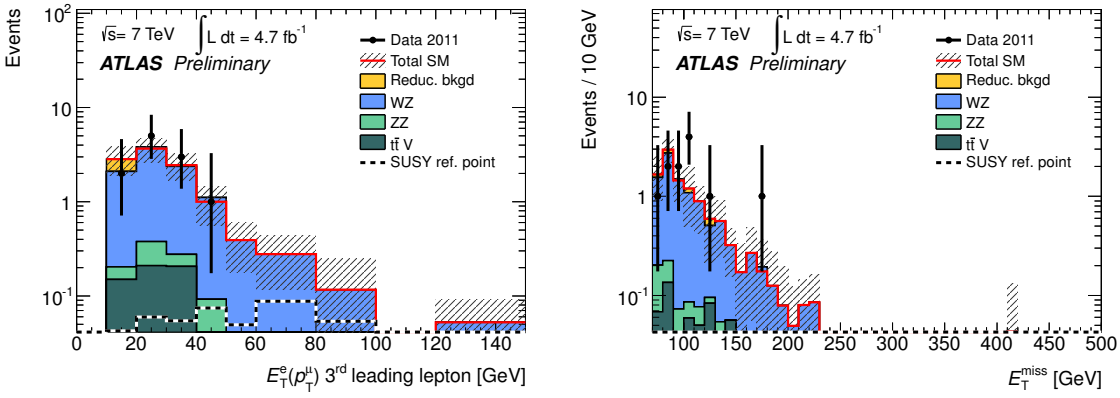

Figure 11: For events in SR2, the p_{T} distribution of the third-leading lepton (left) and the $E_{\mathrm{T}}^{\mathrm{miss}}$ distribution (right) are shown for 2011 data and MC simulation. The grey hatched band represents statistical and systematic uncertainties added in quadrature. The yield for one of the simplified model scenarios, "SUSY ref. point", $(m_{\tilde{\chi}_1^\pm}, m_{\tilde{\chi}_2^0}, m_{\tilde{\ell}_L}, m_{\tilde{\chi}_1^0} = 425,\ 425,\ 250,\ 75\ \mathrm{GeV})$ is also shown for illustration purposes. For this SUSY ref. point, 8.0±0.8 events are expected in SR1a, 6.5±0.6 in SR1b and 0.46±0.05 in SR2. The expected yield for the SUSY ref. point is small in SR2 as this scenario is not rich in on-shell Z bosons.

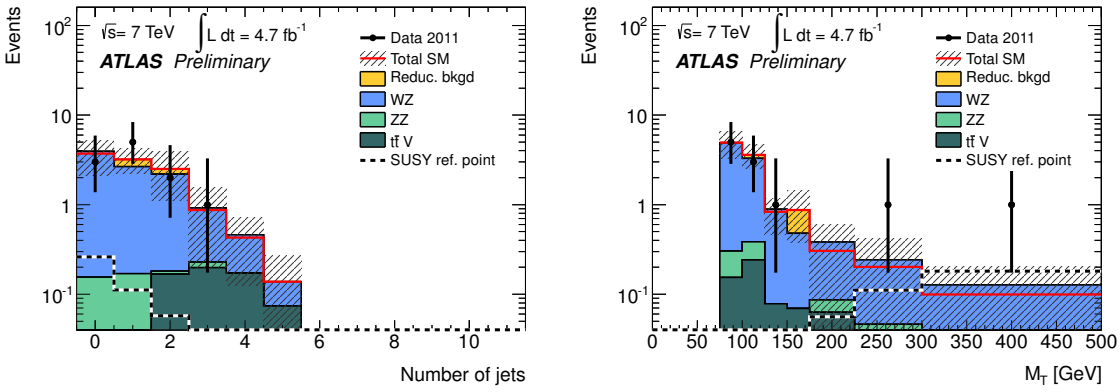

Figure 12: For events in SR2, the jet multiplicity (left) m_{T} (right) distributions are shown for 2011 data and MC simulation. The m_{T} is formed using the $E_{\mathrm{T}}^{\mathrm{miss}}$ and the lepton not forming the best Z candidate. The grey hatched band represents statistical and systematic uncertainties added in quadrature. The yield for one of the simplified model scenarios, "SUSY ref. point", ($m_{\tilde{\chi}_1^\pm}, m_{\tilde{\chi}_2^0}, m_{\tilde{\ell}_L}, m_{\tilde{\chi}_1^0} = 425$, 425, 250, 75 GeV) is also shown for illustration purposes. For this SUSY ref. point, 8.0±0.8 events are expected in SR1a, 6.5±0.6 in SR1b and 0.46±0.05 in SR2. The expected yield for the SUSY ref. point is small in SR2 as this scenario is not rich in on-shell Z bosons.

x

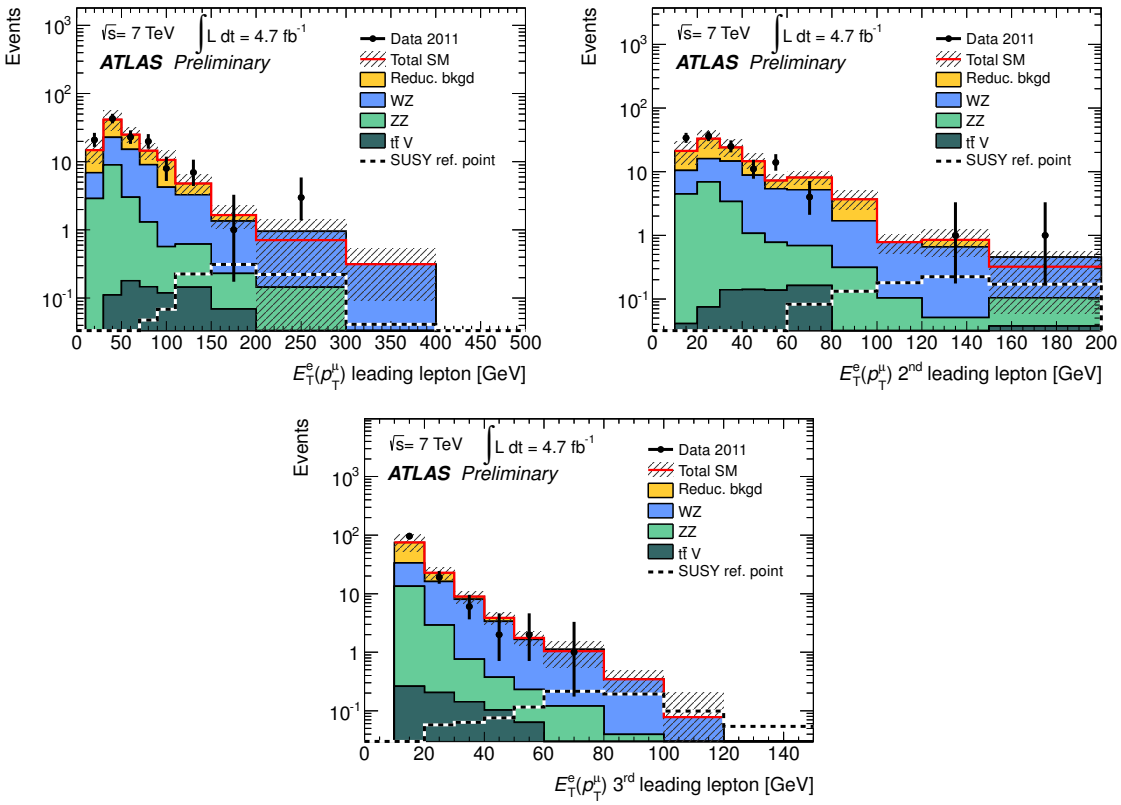

Figure 13: For events in VR1, the p_{T} distributions of the leading (top left), sub-leading (top right) and third-leading (bottom) lepton are shown for 2011 data and MC simulation. The grey hatched band represents statistical and systematic uncertainties added in quadrature.

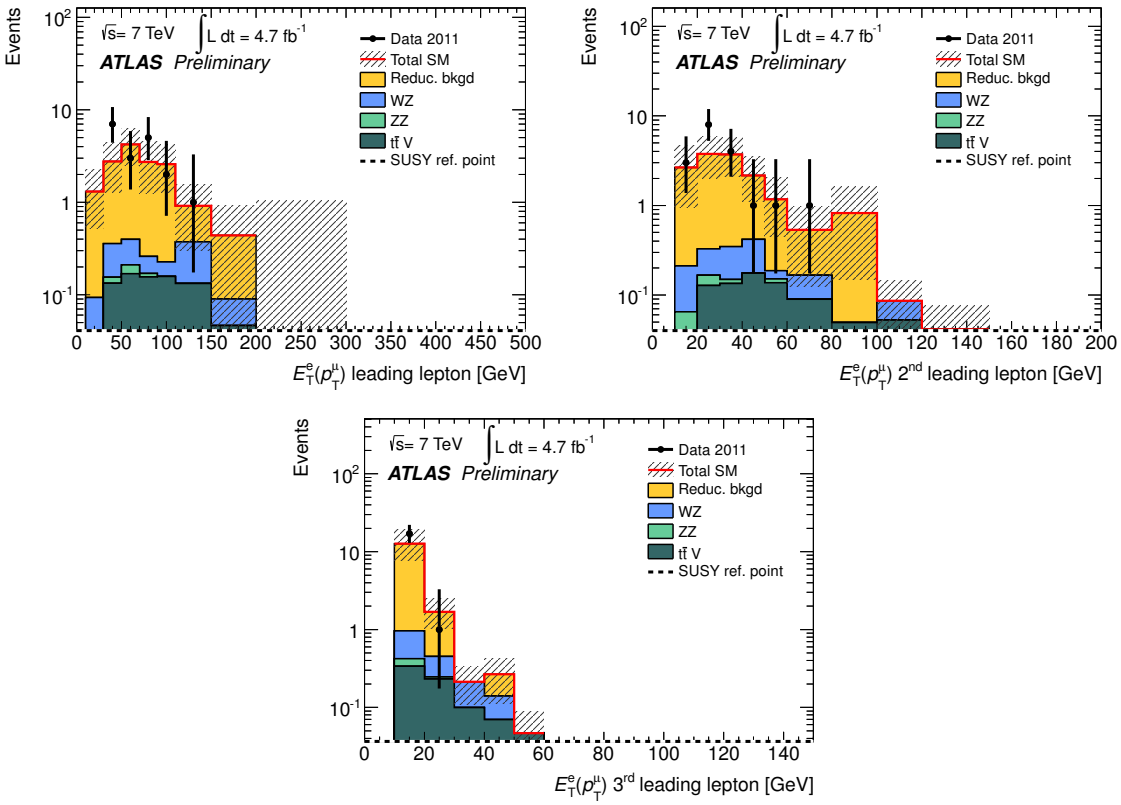

Figure 14: For events in VR2, the p_{T} distributions of the leading (top left), sub-leading (top right) and third-leading (bottom) lepton are shown for 2011 data and MC simulation. The grey hatched band represents statistical and systematic uncertainties added in quadrature.

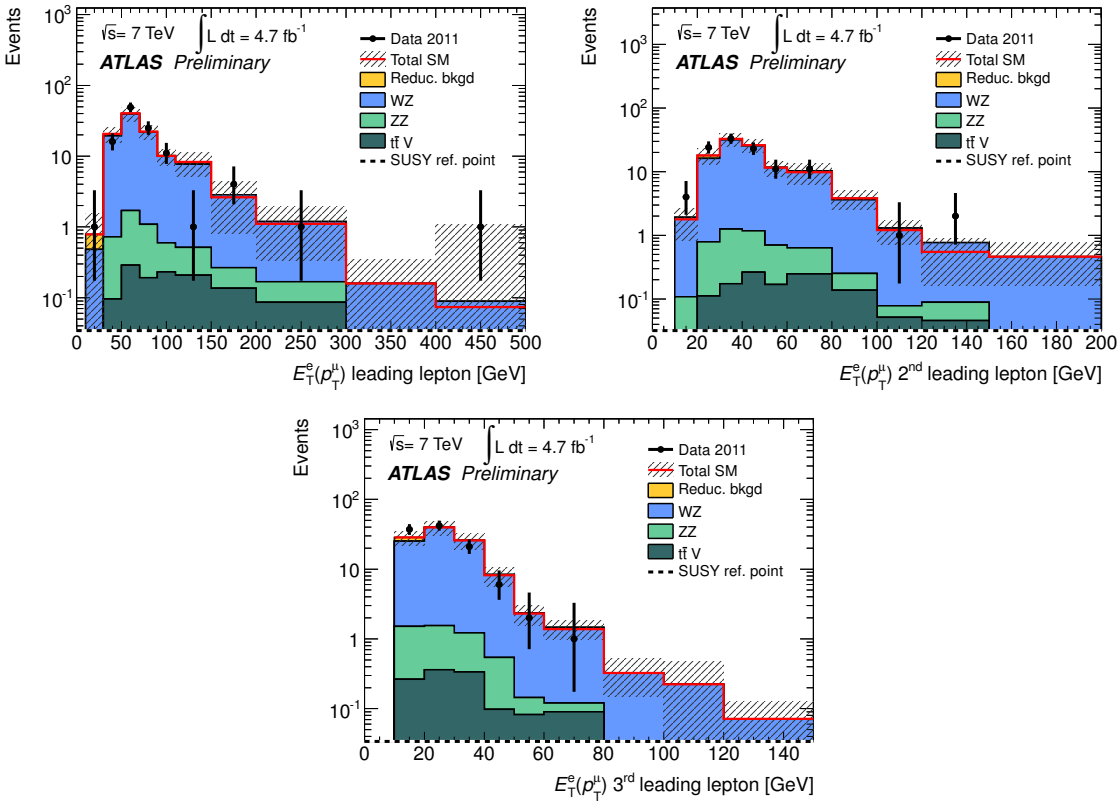

Figure 15: For events in VR3, the p_{T} distributions of the leading (top left), sub-leading (top right) and third-leading (bottom) lepton are shown for 2011 data and MC simulation. The grey hatched band represents statistical and systematic uncertainties added in quadrature.

References

[1] H. Miyazawa, Prog. Theor. Phys. **36** (1966) 1266–1276.

[2] P. Ramond, Phys. Rev. **D3** (1971) 2415–2418.

[3] Y. Golfand, E. Likhtman, JETP Lett. **13** (1971) 323–326.

[4] A. Neveu, J. H. Schwarz, Nucl. Phys. **B31** (1971) 86–112.

[5] A. Neveu, J. H. Schwarz, Phys. Rev. **D4** (1971) 1109–1111.

[6] J. L. Gervais, B. Sakita, Nucl. Phys. **B34** (1971) 632–639.

[7] D. Volkov, V. Akulov, Phys. Lett. **B46** (1973) 109–110.

[8] J. Wess, B. Zumino, Phys. Lett. **B49** (1974) 52.

[9] J. Wess, B. Zumino, Nucl. Phys. **B70** (1974) 39–50.

[10] P. Fayet, Phys. Lett. **B64** (1976) 159.

[11] P. Fayet, Phys. Lett. **B69** (1977) 489.

[12] G. R. Farrar, P. Fayet, Phys. Lett. **B76** (1978) 575–579.

[13] P. Fayet, Phys. Lett. **B84** (1979) 416.

[14] S. Dimopoulos, H. Georgi, Nucl. Phys. **B193** (1981) 150.

[15] K. L. Chan, U. Chattopadhyay, P. Nath, Phys. Rev. **D58** (1998) 096004.

[16] ATLAS Collaboration, Phys. Lett. **B709** (2012) 137.

[17] ATLAS Collaboration, accepted by Phys. Rev. Lett., arXiv:1204.5638, 2012.

[18] CMS Collaboration, SUS-11-016-PAS, 2012.

[19] D0 Collaboration, Phys. Lett. **B680** (2009) 34.

[20] CDF Collaboration, Phys. Rev. Lett. **101** (2008) 251801.

[21] K. Nakamura *et al.* (Particle Data Group), J. Phys. **G37** (2010) 075021.

[22] ATLAS Collaboration, JINST **3** (2008) S08003.

[23] ATLAS uses a right-handed coordinate system with its origin at the nominal interaction point (IP) in the centre of the detector and the z-axis along the beam pipe. The x-axis points from the IP to the centre of the LHC ring, and the y-axis points upward. Cylindrical coordinates (R, ϕ) are used in the transverse plane, ϕ being the azimuthal angle around the beam pipe. The pseudorapidity is defined in terms of the polar angle θ as $\eta = -\ln\tan(\theta/2)$..

[24] A. Djouadi, J.L. Kneur, G. Moultaka, Comput. Phys. Commun. **176** (2007) 426.

[25] J. Alwall, P. Schuster, N. Toro, Phys. Rev. **D79** (2009) 075020.

[26] T. Appelquist, H. Cheng, B. Dobrescu, Phys. Rev. D **64** (2001) 035002.

[27] P. Meade, N. Sieberg, D. Shih, Prog. Theor. Phys Suppl. **177** (2009) 143–158.

[28] J.T. Ruderman, D. Shih, arXiv:1103.6083v1, 2011.

[29] T. Gleisberg *et al.*, JHEP **0902** (2009) 007.

[30] G. Corcella *et al.*, JHEP **0101** (2001) 010.

[31] J. Alwall, M. Herquet, F. Maltoni, O. Mattelaer, T. Stelzer, JHEP **06** (2011) 128.

[32] S. Frixione and B.R. Webber, JHEP **0206** (2002) 029.

[33] M. Mangano *et al.*, JHEP **0307** (2003) 001.

[34] J. M. Campbell, R. K. Ellis, Phys. Rev. **D60** (1999) 113006.

[35] J. M. Campbell, R. K. Ellis, C. Williams, JHEP **07** (2011) 018.

[36] M. Aliev, et al., Comput. Phys. Commun. **182** (2011) 1034.

[37] A. Kardos et al., arXiv:1111.0610, 2011.

[38] J. M. Campbell, R. K. Ellis, arXiv:1204.5678, 2012.

[39] K. Melnikov, F. Petriello, Phys. Rev. **D74** (2006) 114017.

[40] C. Anastasiou *et al.*, Phys. Rev. **D69** (2004) 094008.

[41] J. Pumplin *et al.*, JHEP **0207** (012) 2002.

[42] H. Lai et al, Phys. Rev. **D82** (2010) 074024.

[43] A. Sherstnev and R. S. Thorne, Eur. Phys. J. **C55** (2008) 553575.

[44] M. Bahr *et al.*, Eur. Phys. J. **C58** (2008) 639.

[45] W. Beenakker *et al.*, Nucl. Phys. **B492** (1997) 51–103.

[46] T. Sjostrand, S. Mrenna, P. Skands, JHEP **05** (2006) 026.

[47] GEANT4 Collaboration, Nucl. Instrum. Meth. **A506** (2003) 250–303.

[48] ATLAS Collaboration, Eur. Phys. J **C70** (2010) 823–874.

[49] ATLAS Collaboration, submitted to Eur. Phys. J. C, arXiv:1112.6426, 2011.

[50] ATLAS Collaboration, Eur. Phys. J **C72** (2012) 1909.

[51] ATLAS Collaboration, JHEP **12** (2010) 60.

[52] M. Cacciari, G.P. Salam, G. Soyez, JHEP **04** (2008) 063.

[53] ATLAS Collaboration, ATLAS-CONF-2011-102, https://cdsweb.cern.ch/record/1369219.

[54] ATLAS Collaboration, Eur. Phys. J. **C72** (2012) 1844.

[55] ATLAS Collaboration, Eur. Phys. J. **C71** (2011) 1577.

[56] P. M. Nadolsky *et al.*, Phys. Rev. **D78** (2008) 013004.

[57] A. D. Martin, *et al.*, Eur. Phys. J. **C63** (2009) 189.

[58] M. Botje, *et al.*, arXiv:1101.0538, 2011.

[59] ATLAS Collaboration, Eur. Phys. J. **C71** (2011) 1630.

[60] ATLAS Collaboration, ATLAS-CONF-2011-116, https://cdsweb.cern.ch/record/1376384.

[61] A. L. Read, J. Phys. **G28** (2002) 2693.

[62] G. Cowan, *et al.*, Eur. Phys. J. **C71** (2011) 1554.

[63] ATLAS Collaboration, ATLAS-CONF-2011-155, https://cdsweb.cern.ch/record/1398201.

[64] ATLAS Collaboration, ATLAS-CONF-2012-046, https://cdsweb.cern.ch/record/1448222.